THE JOURNAL OF BIOLOGICAL CHEMISTRY VOL. 292, NO. 6, pp. 2457–2469, February 10, 2017

A Single Amino Acid Mutation Converts (*R*)-5-Diphosphomevalonate Decarboxylase into a Kinase*[S]

Received for publication, August 8, 2016, and in revised form, December 11, 2016 Published, JBC Papers in Press, December 21, 2016, DOI 10.1074/jbc.M116.752535

Kento Motoyama[‡], Hideaki Unno[§], Ai Hattori[‡], Tomohiro Takaoka[¶], Hiroshi Ishikita[¶‖], Hiroshi Kawaide[**], Tohru Yoshimura[‡], and Hisashi Hemmi[‡1]

From the [‡]Department of Applied Molecular Bioscience, Graduate School of Bioagricultural Sciences, Nagoya University, Furo-cho, Chikusa-ku, Nagoya, Aichi 464-8601, the [§]Graduate School of Engineering, Nagasaki University, Bunkyo-machi, Nagasaki, Nagasaki 852-8521, the [¶]Department of Applied Chemistry, University of Tokyo, 7-3-1 Hongo, Bunkyo-ku, Tokyo 113-8654, the [‖]Research Center for Advanced Science and Technology, University of Tokyo, Komaba 4-6-1, Meguro, Tokyo 153-8904, and the [**]Institute of Agriculture, Tokyo University of Agriculture and Technology, Saiwaicho 3-5-8, Fuchu, Tokyo 183-8509, Japan

Edited by Ruma Banerjee

The biosynthesis of isopentenyl diphosphate, a fundamental precursor for isoprenoids, via the mevalonate pathway is completed by diphosphomevalonate decarboxylase. This enzyme catalyzes the formation of isopentenyl diphosphate through the ATP-dependent phosphorylation of the 3-hydroxyl group of (*R*)-5-diphosphomevalonate followed by decarboxylation coupled with the elimination of the 3-phosphate group. In this reaction, a conserved aspartate residue has been proposed to be involved in the phosphorylation step as the general base catalyst that abstracts a proton from the 3-hydroxyl group. In this study, the catalytic mechanism of this rare type of decarboxylase is re-investigated by structural and mutagenic studies on the enzyme from a thermoacidophilic archaeon *Sulfolobus solfataricus*. The crystal structures of the archaeal enzyme in complex with (*R*)-5-diphosphomevalonate and adenosine 5′-*O*-(3-thio)triphosphate or with (*R*)-5-diphosphomevalonate and ADP are newly solved, and theoretical analysis based on the structure suggests the inability of proton abstraction by the conserved aspartate residue, Asp-281. Site-directed mutagenesis on Asp-281 creates mutants that only show diphosphomevalonate 3-kinase activity, demonstrating that the residue is required in the process of phosphate elimination/decarboxylation, rather than in the preceding phosphorylation step. These results enable discussion of the catalytic roles of the aspartate residue and provide clear proof of the involvement of a long predicted intermediate, (*R*)-3-phospho-5-diphosphomevalonate, in the reaction of the enzyme.

In the classical mevalonate (MVA)[2] pathway, diphosphomevalonate decarboxylase (DMD) catalyzes the conversion of (*R*)-5-diphosphomevalonate (MVA-5-PP) into isopentenyl diphosphate (IPP), which acts as a fundamental active unit for isoprenoid biosynthesis (1). The enzyme requires ATP and Mg^{2+} for the reaction, which is normal with kinases. In fact, DMD shows homology with the members of the GHMP (galactokinase, homoserine kinase, mevalonate kinase, and phosphomevalonate kinase) kinase superfamily. The widely accepted reaction mechanism of DMD (Fig. 1*A*) is as follows (2). 1) The enzyme transfers the γ-phosphate group of ATP to the 3-hydroxyl group of MVA-5-PP to produce a hypothetical intermediate, (*R*)-3-phospho-5-diphosphomevalonate (MVA-3-P-5-PP). 2) DMD catalyzes the elimination of the 3-phosphate group of the intermediate, generating a 3° carbocationic intermediate. 3) Decarboxylation occurs with the transfer of electrons to the positive charge on C3, which results in the formation of IPP. When catalyzing decarboxylation, general decarboxylases (3) utilize various functional groups in their substrates (or the intermediates covalently bonded with coenzymes) as an "electron sink," which exists proximal to a carboxyl group and can temporarily accept electrons generated from decarboxylation, such as a β-carbonyl group (*e.g.* malonyl-CoA decarboxylase (4)), an α-amino group activated by pyridoxal phosphate (*e.g.* L-aromatic amino acid decarboxylase (5)), an α-carbonyl group attached by thiamine diphosphate-ylide (*e.g.* pyruvate decarboxylase (6)) and an α,β-double bond connected to a flavin derivative (*e.g.* ferulic acid decarboxylase (7)). DMD and its recently discovered homolog, phosphomevalonate decarboxylase (8, 9), are limited examples of the decarboxylases that utilize the positive charge of a carbocation as an acceptor of electrons. The involvement of the carbocation intermediate, however, remains controversial, and the concerted elimination of the phosphate and carboxyl groups has

* This work was supported in part by Japan Society for the Promotion of Science KAKENHI Grants 25108712 and 16K14882 (to H. H.) and Grants 15H00864, 26105012, and 26711008 (to H. I.), Takeda Science Foundation (to H. H.), Japan Science and Technology Agency CREST (to H. I.), Materials Integration for Engineering Polymers of Cross-ministerial Strategic Innovation Promotion Program (SIP) (to H. I.), and the Interdisciplinary Computational Science Program in CCS, University of Tsukuba. The authors declare that they have no conflicts of interest with the contents of this article.

[S] This article contains supplemental Fig. S1 and Tables S1–S3.

The atomic coordinates and structure factors (codes 5GMD and 5GME) have been deposited in the Protein Data Bank (http://wwpdb.org/).

[1] To whom correspondence should be addressed. Tel.: 81-52-789-4134; Fax: 81-52-789-4120; E-mail: hhemmi@agr.nagoya-u.ac.jp.

[2] The abbreviations used are: MVA, mevalonate; ATPγS, adenosine 5′-*O*-(3-thio)triphosphate; DMD, diphosphomevalonate decarboxylase; ESI, electron spray ionization; IP, isopentenyl phosphate; IPP, isopentenyl diphosphate; M3K, mevalonate 3-kinase; MVA-3-P, 3-phosphomevalonate; MVA-3-P-5-PP, (*R*)-3-phospho-5-diphosphomevalonate; MVA-5-P, 5-phosphomevalonate; MVA-5-PP, 5-diphosphomevalonate; MVK, mevalonate kinase; PMK, phosphomevalonate kinase; SsoDMD, *S. solfataricus* DMD; TacM3K, *T. acidophilum* M3K; PDB, Protein Data Bank.

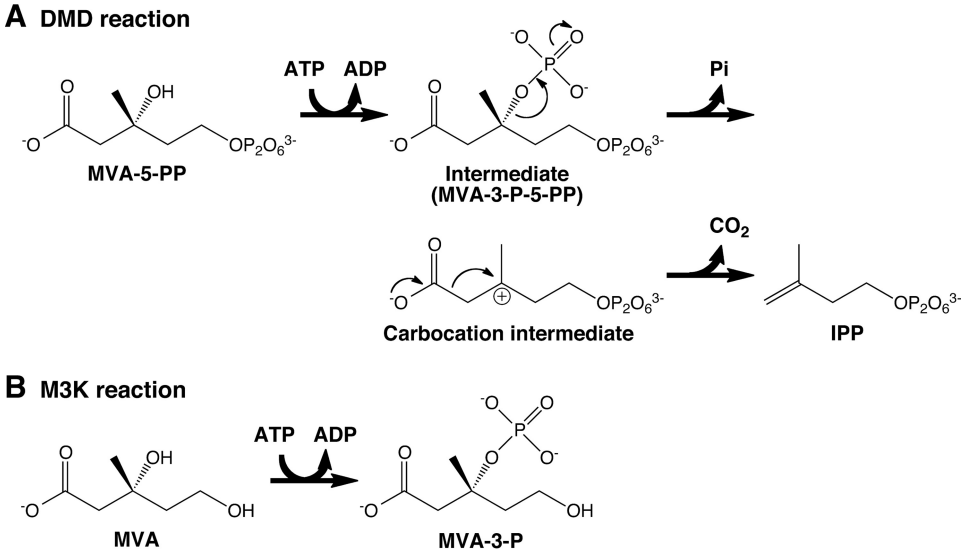

FIGURE 1. **Reaction mechanisms of DMD (*A*) and M3K (*B*).**

also been proposed (10). In addition, although Dhe-Paganon *et al.* (11) have reported the detection of a probable 3-phosphorylated product from the reaction of DMD with the 6-fluorinated analog of MVA-5-PP, we are not aware of any direct demonstrations that the intermediate MVA-3-P-5-PP is formed.

The crystal structures of DMD have been solved with eukaryotic enzymes from *Saccharomyces cerevisiae* (12), *Trypanosoma brucei* (13), mice, and humans (14); with bacterial enzymes from *Staphylococcus aureus* (13), *Streptococcus pyogenes*, *Legionella pneumophila*, and *Staphylococcus epidermidis* (15, 16); and with an archaeal enzyme from *Sulfolobus solfataricus* (17). Among them, only those of DMD from *S. epidermidis* were solved in complex forms with the substrates or inhibitors (Fig. 2*A*) and have thus provided persuasive information about the catalytic mechanism of the enzyme. Based on real (15, 16) or modeled (13, 14) substrate-complex structures, and also on the results from a mutagenic study (18), an aspartate residue, which resides in the proximity of the 3-hydroxyl group of MVA-5-PP, was anticipated to be the base catalyst that abstracts a proton from the hydroxyl group to induce the phosphotransfer reaction from ATP (Fig. 2*B*). The aspartate residue, such as Asp-283 in *S. epidermidis* DMD and Asp-302 in *S. cerevisiae* DMD, is conserved in all DMDs and phosphomevalonate decarboxylases. The replacement of the aspartate residue with alanine or asparagine significantly reduces enzyme activity, according to a mutagenic study with *S. cerevisiae* DMD (10^3- and 10^5-fold decrease by D302N and D302A mutation, respectively (18)). Krepkiy and Miziorko (18) concluded that the reduction of activity supports the role of the aspartate residue as the base catalyst.

However, the mutagenic study focused on loss of product formation, rather than monitoring the fate of the substrate, so it is not clear whether any steps of the reaction could proceed. The structures of mevalonate 3-kinase (M3K) from a thermoacidophilic archaeon *Thermoplasma acidophilum*, which

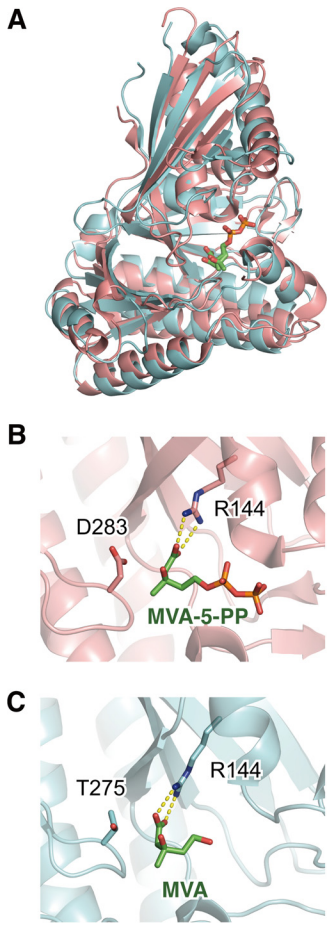

FIGURE 2. **Substrate-complex structures of DMD and M3K.** *A*, superposed structures of DMD (MVA-5-PP complex, PDB code 4DU7) from *S. epidermidis* and M3K (MVA complex, PDB code 4RKS) from *T. acidophilum*. DMD (*pink*) and M3K (*light blue*) are shown as *ribbon* figures. MVA-5-PP in DMD and MVA in M3K are shown as *stick* figures. *B* and *C*, active site structures of DMD (*B*) and M3K (*C*). Residues (Arg-144 and Asp-283 in DMD and Arg-144 and Thr-275 in T3K) and the ligand molecules are shown as *stick* figures. The viewing directions of *B* and *C* are in accordance.

TABLE 1
Data collection and refinement statistics
Numbers in parentheses are for the highest shell.

Crystal type	SsoDMD·ATPγS·MVA-5-PP	SsoDMD·ADP·MVA-5-PP
Data collection and processing statistics		
Beamline	BL-17A	AR-NW12A
Space group	*H*32	*H*32
Unit cell dimension		
$a = b$ (Å)	151.2	151.3
c (Å)	104.4	104.4
Wavelength (Å)	0.980	1.000
Resolution (Å)	50.0–1.50 (1.53–1.50)	27.8–1.70 (1.79–1.70)
Measured	72,125	50,194
Redundancy	10.0 (10.1)	15.2 (15.2)
$I/\sigma I$	37.1 (5.3)	23.0 (5.8)
Completeness (%)	99.2 (100)	99.8 (100)
R_{merge}[a] (%)	6.4 (53.2)	7.2 (45.2)
Refinement statistics		
Resolution	48.5–1.50	27.8–1.70
Protein molecules/asymmetric unit	1	1
Protein atoms	2,614	2,597
Ligand molecules		
AMP	1	1
ATPγS	1	0
ADP	0	1
MVA-5-PP	1	1
Sulfate	2	2
Ligand atoms	83	79
Water molecule	243	257
B-factors		
Protein	20.3	27.7
Ligand	36.3	43.4
Water	28.0	34.5
R_{work}/R_{free}(%)	16.5/19.2	16.9/20.2
Root mean square deviations		
Bond lengths (Å)	0.031	0.026
Bond angles (°)	2.956	2.593

[a] $R_{merge} = 100\Sigma|I - \langle I\rangle|/\Sigma I$, where I is the observed intensity and $\langle I\rangle$ is the average intensity of multiple observations of symmetry-related reflections.

were recently solved by Vinokur *et al.* (Fig. 2*A*) (19), cast new light on this question. The enzyme shows high homology with DMD, but it catalyzes only the phosphorylation of MVA without decarboxylation (Fig. 1*B*) to produce (*R*)-3-phosphomevalonate (MVA-3-P) as an intermediate in the recently discovered *Thermoplasma*-type modified MVA pathway (20, 21). In the active site, the DMD homolog has neither an aspartate residue at the conserved position nor any residues that could abstract a proton from the 3-hydroxyl group of the substrate. M3K has a conserved threonine residue at the site corresponding to the aspartate of DMD (Fig. 2*C*). The replacement of the threonine with alanine did not significantly affect enzyme activity (19). Such information suggested a new catalytic mechanism for DMD, in which the conserved aspartate is likely involved in the decarboxylation step, rather than in the preceding phosphorylation step that also exists in the reaction of M3K.

In this study, we solved the crystal structures of DMD from the hyperthermophilic archaeon *S. solfataricus* (SsoDMD) in the substrate-complex forms. Energetic calculation based on one of the complex structures demonstrated that it is unlikely that the 3-hydroxyl group of MVA-5-PP is deprotonated, particularly by the conserved aspartate residue, Asp-281. Therefore, we performed site-directed mutagenesis on SsoDMD and also on M3K from *T. acidophilum* (TacM3K). The results from the structural and mutagenic studies suggest the possible functions of the aspartate residue via the reaction of DMD.

Results

Structural Analyses of SsoDMD in Complex with the Substrates—We recently have reported the X-ray crystallographic structures of substrate-free SsoDMD (17). Here, we succeeded in solving the structures of SsoDMD in complex with ATPγS and MVA-5-PP (the complex SsoDMD·ATPγS·MVA-5-PP) at a 1.5 Å resolution, and with ADP and MVA-5-PP (SsoDMD·ADP·MVA-5-PP) at a 1.7 Å resolution. Data collection and refinement statistics are summarized in Table 1. The overall structures are similar to those of the substrate-free SsoDMD structures, with the exception of the partial uncoiling of the α1-helix and a slight movement of the β7/α1-loop toward the cleft (Fig. 3, *A* and *B*). These structural changes help the cleft structure adapt to ligand binding; for example, the shift of Tyr-72 creates a pocket that can accommodate either ATPγS or ADP. The changes are, however, in sharp contrast to the dynamic movement of the conserved "P-loop" (corresponding to the β8/α2-loop of SsoDMD, which moves little through ligand binding) observed in the complex structures of *S. epidermidis* DMD (15). In the complex structure of SsoDMD·ATPγS·MVA-5-PP, the uncoiling of the α1-helix is likely stabilized by newly formed hydrogen bonds between Arg-62 and Glu-68, between Asp-67 and Lys-70, and between Glu-71 and Arg-75 (Fig. 3*C*). Meanwhile, in the complex structure of SsoDMD·ADP·MVA-5-PP, the former two bonds are absent, and Glu-68 coordinates with the 2′-OH and 3′-OH of ADP (Fig. 3*D*). ATPγS and ADP are coordinated by Ser-94 at N-6 of the adenine moiety and by Ser-107 at β-phos-

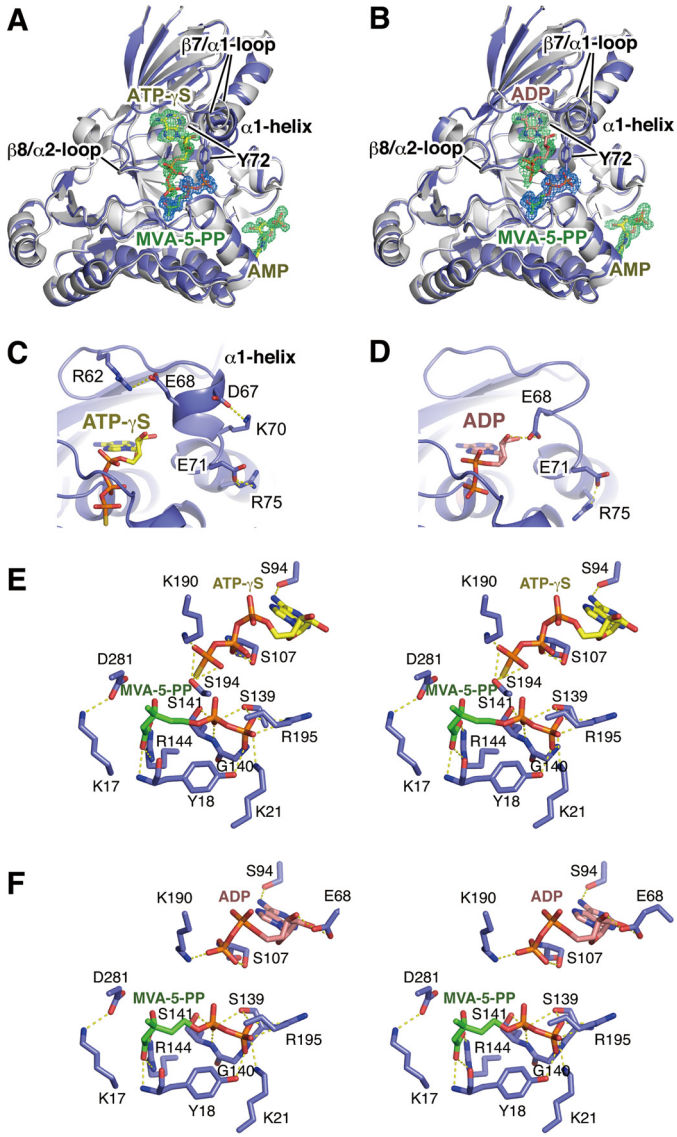

FIGURE 3. **Substrate·complex structures of SsoDMD.** *A* and *B*, complex structures (monomer, colored in *deep blue*) of SsoDMD·ATPγS·MVA-5-PP (*A*) and SsoDMD·ADP·MVA-5-PP (*B*) are superimposed with a substrate-free structure (PDB code 4Z7Y, *gray*). MVA-5-PP (*green*), ATPγS (*yellow*), ADP (*pink*), and AMP (*yellow*) molecules that are bound to SsoDMD and the Tyr-72 residue are represented by *stick* models. The $F_o - F_c$ omit electron density maps for ligands bound to SsoDMD are shown as *mesh*. The omit maps are contoured at 2.2σ. *C* and *D*, hydrogen-bonding interactions around α1-helix in SsoDMD·ATPγS·MVA-5-PP (*C*) and SsoDMD·ADP·MVA-5-PP (*D*). The *dashed lines* denote hydrogen bonds. *E* and *F*, stereo view of the active site structures of SsoDMD·ATPγS·MVA-5-PP (*E*) and SsoDMD·ADP·MVA-5-PP (*F*). The ligands and the amino acid residues involved in the ligand binding with hydrogen-bonding interactions are represented as *stick* models. Probable hydrogen bond-forming interactions (in proximity less than ~3 Å) are indicated by *yellow dotted lines*.

phate (Fig. 3, *E* and *F*). Lys-190 coordinates with the γ-thiophosphate and β-phosphate of ATPγS and ADP, respectively. Ser-194 also coordinates with the γ-thiophosphate of ATPγS. It should be noted that the Mg^{2+} ion is absent in the structures even though ~10 mM $MgCl_2$ was contained in the drops for crystallization. The ion is considered to interact with the triphosphate group of ATP to stimulate phosphotransfer, as expected by Barta *et al.* (15) based on the structure of phosphomevalonate kinase (PMK), which is homologous with DMD. The residues involved in the binding of MVA-5-PP are identical between the two complexes and are basically similar to those observed in the complex structures of *S. epidermidis* DMD (15, 16). The carboxyl group of MVA-5-PP is coordinated with Arg-144 and with the main chain of Tyr-18; the α-phosphate is coordinated with Ser-139 and Ser-141; and the β-phosphate is coordinated with Tyr-18, Lys-21, Ser-139, Arg-195 and the main chain of Gly-140 (Fig. 3, *E* and *F*). The distance between the 3-hydroxyl group of MVA-5-PP and the phosphorus atom of the γ-thiophosphate group of ATPγS is 5.9 Å, which seems too far to enable phosphotransfer between them. Because Lys-190, which coordinates with the γ-thiophosphate group of ATPγS, is a highly flexible residue with a relatively high B-factor, it presumably plays a role in guiding the γ-phosphate group of ATP to an appropriate position for phosphotransfer. The Asp-281 residue, which forms an ion pair with Lys-17 at a distance of 2.8 Å, juxtaposes the 3-hydroxyl group of MVA-5-PP at a distance of ~3.5 Å. It is noteworthy that the carboxyl and 3-hydroxyl groups of MVA-5-PP take a "gauche" conformation in the complex structures of SsoDMD and also in those of *Streptococcus pneumoniae* DMD, although a previous study (22) has shown that the elimination of these groups occurs in an anti-manner via the DMD reaction.

Other than the ligands binding in the catalytic cleft, MVA-5-PP and either ATPγS or ADP, there is an electron density per each monomer of DMD, which can be attributed to a molecule of AMP, although it is probably derived from the disorder of the terminal phosphate group(s) of either ATPγS or ADP (Fig. 3, *A* and *B*). A disulfide-bonded dimer is the expected physiological quaternary structure of SsoDMD (17). In the crystals, three dimers are related to a 3-fold crystallographic symmetry axis, although there is one monomer in the asymmetric unit. The binding positions of AMP are at the packing interface between dimers; however, AMP seems binding tightly with only one of the dimers through several hydrogen bonds with a Lys and two Glu residues, although it just interacts with a main chain carbonyl group of the other dimer (data not shown). Moreover, the direct interaction between the dimers does not change largely by ligand binding. Therefore, the binding of AMP is considered not to affect the quaternary structure of SsoDMD, although the physiological meaning of the AMP-binding site remains elusive.

Theoretical Analysis—Based on the crystal structure of SsoDMD·ATPγS·MVA-5-PP, the calculated protonation pattern of the titratable sites indicated that the triphosphoric part of ATP was singly protonated ($[H\text{-}PPP]^{3-}$) and that the diphosphoric part of MVA-5-PP was also singly protonated ($[H\text{-}PP]^{2-}$) in SsoDMD. pK_a was calculated to be 26.5 for the 3-hydroxyl group of MVA-5-PP in the SsoDMD protein environment. The carboxyl and diphosphate groups of MVA-5-PP and the triphosphate group of ATP contributed to increases in the calculated pK_a of 8.4, 4.7, and 6.5, respectively (Table 2). The possible binding of Mg^{2+} at the triphosphate group of ATP may cause a decrease in the pK_a for the 3-hydroxyl group of MVA-5-PP. At the same time, however, the Mg^{2+} binding would cause deprotonation of the singly protonated triphosphate group (*i.e.* $[H\text{-}PPP]^{3-}$), partially compensating for the influence of cationic Mg^{2+}. It seems likely that pK_a for the

TABLE 2
Contribution of residues to the calculated pK_a shifts of 3-hydroxyl group of MVA-5-PP in SsoDMD relative to the bulk solvent (in pK_a units)

Sites	Contribution to calculated pK_a (3-hydroxyl group)		
	Side chain	Main chain	Total
Decreasing pK_a (3-hydroxyl group)			
Lys-17	−4.1	−0.5	−4.6
Lys-21	−1.7	−0.1	−1.8
Arg-136	−0.6	0.1	−0.5
Ser-141	−0.3	−0.3	−0.6
Arg-144	−4.0	−0.2	−4.2
Lys-190	−2.2	−0.1	−2.3
Arg-195	−1.0	0.0	−1.0
Arg-211	−1.7	0.0	−1.7
His-287	−2.1	0.0	−2.1
Increasing pK_a (3-hydroxyl group)			
Tyr-18	−0.1	1.0	0.9
Asp-40	0.3	0.1	0.4
Asp-180	1.3	−0.1	1.2
Asp-281	3.2	−0.8	2.4
Carboxyl group of MVA-5-PP			8.4
Diphosphate group of MVA-5-PP			4.7
Triphosphate group of ATP			6.5

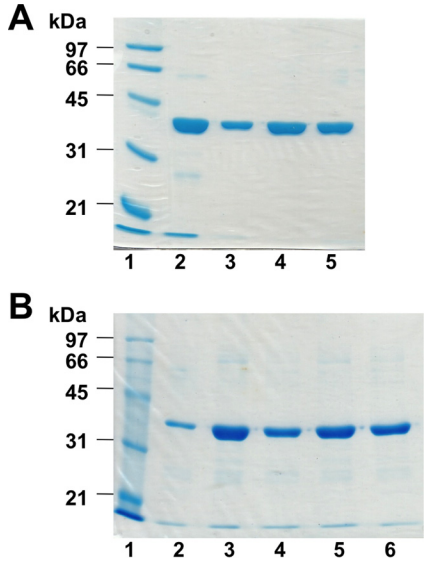

FIGURE 4. **SDS-PAGE analysis of the purified enzymes.** *A*, wild type and Asp-281 mutants of SsoDMD. *Lane 1*, molecular marker; *lane 2*, wild type (37.0 kDa); *lane 3*, D281N; *lane 4*, D281T; and *lane 5*, D281V. *B*, wild type, Thr-275 single, and Leu-18/Thr-275 double mutants of TacM3K. *Lane 1*, molecular marker; *lane 2*, wild type (35.2 kDa); *lane 3*, T275D; *lane 4*, T275E; *lane 5*, L18K/T275D; and *lane 6*, L18K/T275E. The proteins were separated on 12.5% SDS-PAGE.

3-hydroxyl group is sufficiently high even in the presence of Mg^{2+}. In contrast, Asp-281 contributed to an increase in the calculated pK_a of only 2.4. Notably, the carboxyl oxygen atom of Asp-281 was 3.4 Å away from the 3-hydroxyl oxygen atom of MVA-5-PP. It seems unlikely that Asp-281 abstracts a proton from the 3-hydroxyl group of MVA-5-PP, unless the two O moieties form a hydrogen bond, and this was obviously not the case in the geometry of the crystal structure (Fig. 3*E*).

Mutation Analyses of SsoDMD—To examine the role of the conserved aspartate residue, we constructed the following three Asp-281 mutants of SsoDMD: D281N, D281T, and D281V. It should be noted that the threonine mutant D281T mimics the active site of TacM3K because Thr-275 exists in TacM3K at the corresponding position with that of Asp-281 in SsoDMD. The mutants were recombinantly expressed in *Escherichia coli*, purified by affinity chromatography (Fig. 4*A*), and used in a radio-TLC enzyme assay (Fig. 5*A*). The products of the mutants were different from those of the wild type SsoDMD, particularly when the native substrate of DMD, [2-^{14}C]MVA-5-PP, was used. The DMD activity, which yields IPP from MVA-5-PP in the presence of ATP, was observed only with the wild type and with the D281N mutant. The retention of significant DMD activity by the mutant lacking the acidic residue clearly refuted the role of Asp-281 as the general base catalyst. Interestingly, a faint radioactive spot with an R_f value that was smaller than those of IPP and MVA-5-PP was observed in proximity to the origin of the normal phase TLC analysis of the D281N reaction products, which suggested high polarity for the product. The radio-TLC analysis of the products from the reaction with the D281T or D281V mutants demonstrated a complete loss of the DMD activity from both mutants, although the substrate MVA-5-PP was almost completely converted into a highly polar compound, which formed a dense spot with an R_f similar to that of the faintly observed spot in the analysis of the D281N reaction products. We also detected unexpected differences in the products from (*R*)-5-phosphomevalonate (MVA-5-P) among the wild type and mutant enzymes. The wild type enzyme produced IPP from MVA-5-P and ATP. This result implies the following two possibilities: 1) SsoDMD promiscuously decarboxylates MVA-5-P to form isopentenyl phosphate (IP) and then catalyzes the IP kinase reaction, or 2) SsoDMD has additional PMK activity. The presence of a faint spot corresponding to IP, however, suggests that the former option is more likely. Both the MVA-5-P decarboxylase and IP kinase activities of SsoDMD are considered to be only secondary because a major part of MVA-5-P remained unreacted even though an excess amount of the enzyme was added for reaction in this experiment. In contrast, the D281N mutant converts MVA-5-P into an unknown product with an R_f value that is similar to the previously reported R_f value of 3,5-bisphosphomevalonate (20). D281T and D281V did not catalyze the conversion of MVA-5-P. A detailed study of the intriguing properties of D281N will be reported elsewhere in the future.

We were interested in the highly polar products from MVA-5-PP formed by the reaction with D281T and D281V because they were considered to be important to an understanding of the catalytic mechanism of SsoDMD. Because the amount of the enzymes used for the assay was high enough to make the secondary enzyme activities be detected, gradually varied amounts of the D281T and D281V mutants were used for the reaction with ^{14}C-labeled MVA-5-PP to compare their activities with that of the wild type enzyme (Fig. 6). The substrate conversion rates estimated from the radiolabeled spots indicated that the activities of D281T and D281V were ~10% that of wild type SsoDMD. In addition to this rough estimation of enzyme activity from the radio-TLC analysis, we performed the kinetic analyses of the mutants by a colorimetric assay that couples ADP production with the reactions of pyruvate kinase and lactate dehydrogenase and detects the decrease in the absorbance of NADH. The K_m values of the wild type, D281T, and D281V for (*RS*)-MVA-5-PP were 37.2, 51.1, and 30.9 μM, respectively, indicating that their affinities for the substrate are similar. However, the k_{cat} values of the D281T and D281V

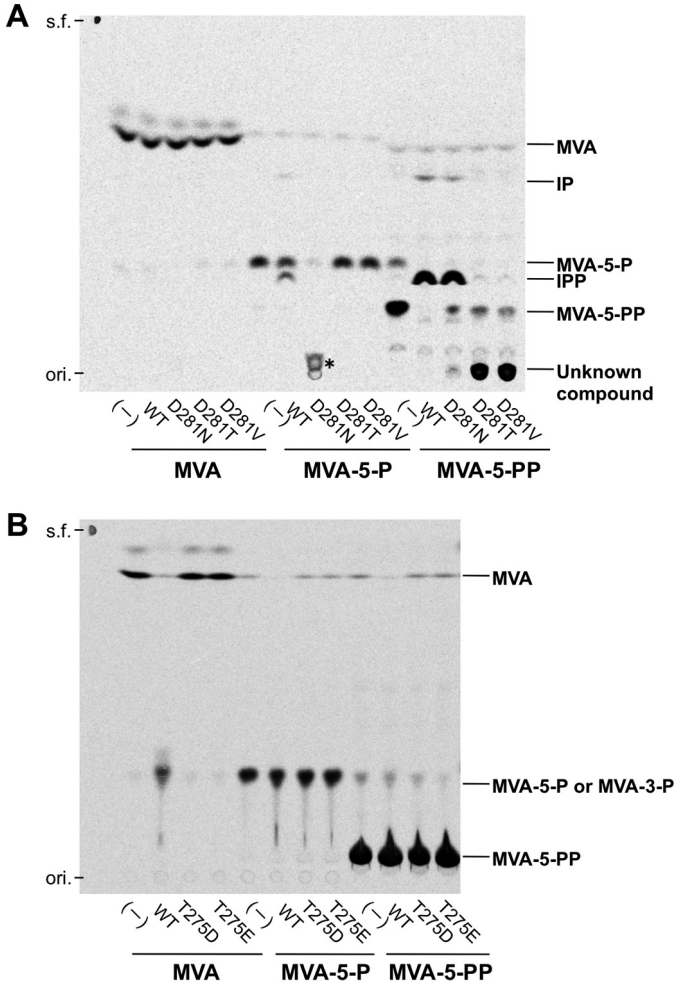

FIGURE 5. **Radio-TLC analyses of the products of the wild type and mutants of SsoDMD (*A*) and TacM3K (*B*).** The *asterisk* indicates an unknown product from the reaction with MVA-5-P and the D281N mutant, which seems distinct from unknown compounds synthesized by the reaction with MVA-5-PP and the D281T or D281V mutant. *ori.*, origin; *s.f.*, solvent front.

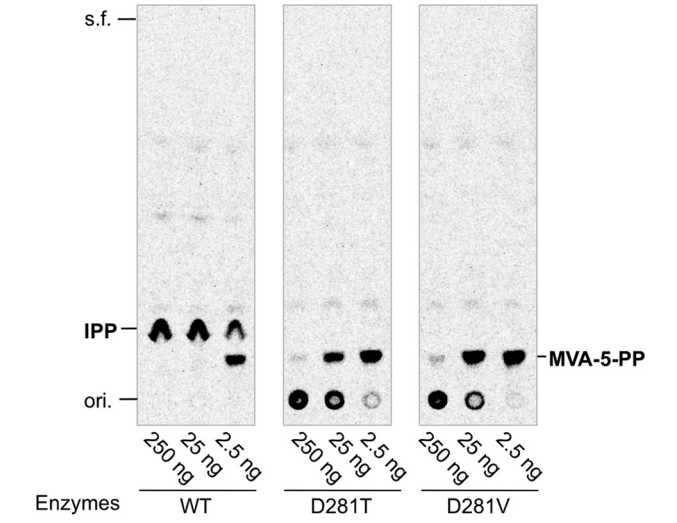

FIGURE 6. **Semi-quantitative radio-TLC assays of the wild type SsoDMD and the D281T and D281V mutants.** 2.5, 25, or 250 ng (0.068, 0.68, and 6.8 pmol, respectively) of each enzyme was reacted for 15 min at 60 °C with 25 pmol of [2-^{14}C]MVA-5-PP in the presence of ATP and Mg^{2+}. *ori.*, origin; *s.f.*, solvent front.

mutants were 8.09×10^{-3} and 6.21×10^{-3} s^{-1}, respectively, which are significantly lower than that of the wild type SsoDMD of 1.06 s^{-1}. Thus, the catalytic efficiencies of the mutants were below 1% that of wild type.

Structural Determination of the Products from the D281T and D281V Mutants—To analyze the chemical structure of the highly polar products from the reaction of the D281T and D281V mutants of SsoDMD, [U-^{13}C]MVA-5-PP was enzymatically synthesized from [U-^{13}C]MVA. In the presence of ATP and Mg^{2+}, purified *S. solfataricus* mevalonate kinase (MVK) and PMK were reacted with the 100% ^{13}C-enriched substrate. As a result, the reaction yielded an approximate 1:1 mixture of MVA-5-P and MVA-5-PP (data not shown). After removal of the enzymes, the D281T mutants of SsoDMD and ATP were added to the reaction mixture to perform an additional reaction. Finally, NMR analysis was conducted after the removal of the enzyme (Fig. 7, Table 3, and supplemental Fig. S1). By the reaction with D281T, a quartet doublet signal emerged at 78.17 ppm, in tandem with a decrease in the C3 signal of MVA-5-PP at 70.88 ppm (Fig. 7, *A* and *B*). The chemical shift of the signal was in good agreement with the reported chemical shift of the C3 signal of the product from TaM3K, MVA-3-P (20). An additional hyperfine coupling associated with its peaks was considered to be the result of two-bond ^{13}C-^{31}P coupling, as observed in the C3 signal of MVA-3-P. These data suggested that the D281T mutant catalyzes the 3-phosphorylation of MVA-5-PP to yield MVA-3-P-5-PP. Some other obvious changes were found between the spectra of the reacted samples with or without D281T, at the signals of C1, C2, C4, and C6 (Figs 7, *C–J*). Near the doublet signal of C1 of MVA-5-PP at 180 ppm, a smaller doublet signal emerged at 179 ppm. The peak number of the quartet C4 signal of MVA-5-PP at 41.24 ppm was increased after the reaction with D281T. A doublet signal came into existence at 25.3 ppm, which approximated the doublet C6 signal of MVA-5-PP at 25.7 ppm. The NMR analysis of the product from the reaction of the D281V mutant gave almost the same results (Table 3).

The electron spray ionization (ESI)-MS analyses of the products of the D281T and D281V mutants were performed in the negative mode using the direct infusion method (Fig. 8). In the MS profile of the sample after the reaction with the non-labeled substrates and the D281T mutant, an ion peak with an *m*/*z* of 387.2, which was absent from the MS profile of the sample from the reaction without the mutant, was observed (Fig. 8, *A* and *B*). The *m*/*z* value corresponds well with the negative ion from MVA-3-P-5-PP. The MS/MS analysis of the ion gave fragment ions with *m*/*z* values of 369.0, 288.9, and 244.8 and were supposedly derived from $[M - H_2O - H]^-$, $[M - H_3PO_4 - H]^-$, and $[M - H_3PO_4 - CO_2 - H]^-$, respectively (Fig. 8*C*). For further confirmation, samples for MS analysis were prepared with the same protocol, with the exception of using [U-^{13}C]MVA as a starting material. The MS profile of the sample after the reaction with D281T gave an ion with an *m*/*z* of 393.0, which was 6 units larger than the ion above and corresponded well with the negative ion from [U-^{13}C]MVA-3-P-5-PP (Fig. 8, *D* and *E*). The MS/MS analysis of the ion yielded fragment ions with *m*/*z* values of 374.8, 294.9, and 249.8, which were likely derived from $[M - H_2O - H]^-$, $[M - H_3PO_4 -$

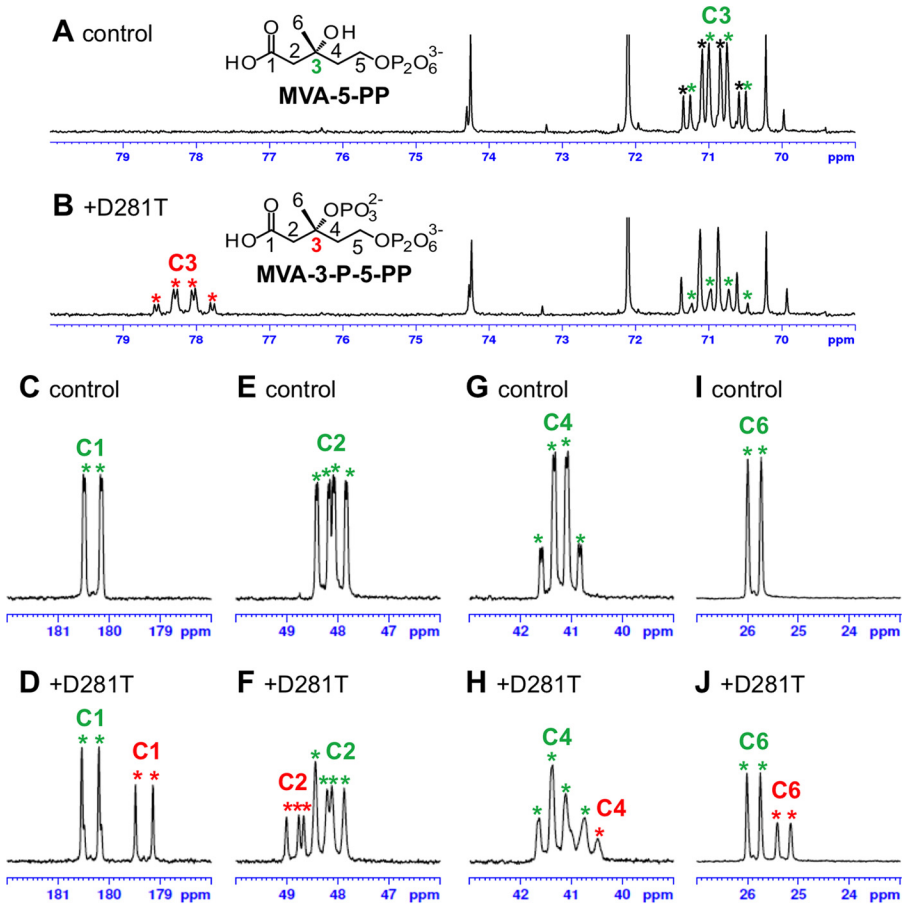

FIGURE 7. **^{13}C NMR analysis of the product of the D281T mutant.** Parts of the ^{13}C NMR spectra after reaction without (*A, C, E, G,* and *I*) or with (*B, D, F, H,* and *J*) the D281T mutant are shown. *Green asterisks* indicate the indistinguishable signals of [U-^{13}C]MVA-5-P and [U-^{13}C]MVA-5-PP, which are derived from the conversion of [U-^{13}C]MVA by MVK and PMK from *S. solfataricus*. *Black asterisks* in *A* represent the signals of [U-^{13}C]MVA-5-P, which are distinguishable from those of [U-^{13}C]MVA-5-PP indicated by *green asterisks*. *Red asterisks* indicate the signal of the product of the D281T mutant. The spectra corresponding to the signals of C3 (*A* and *B*), C1 (*C* and *D*), C2 (*E* and *F*), C4 (*G* and *H*), and C6 (*I* and *J*) of MVA-5-PP and the new product are shown. The reaction with the D281V mutant gave almost the same results as those from the reaction with D281T (data not shown).

TABLE 3
^{13}C NMR data for [U-^{13}C]MVA-5-PP and the SsoDMD mutant product from [U-^{13}C]MVA-5-PP

Compound	Carbon no.	Chemical shift	Coupling pattern[a]
[U-^{13}C]MVA-5-PP	1	180.3	d
	2	48.1	dd
	3	70.9	q
	4	41.2	q
	5	62.4	d
	6	25.7	d
Product of the D281T mutant from [U-^{13}C]MVA-5-PP	1	179.3	d
	2	~49	m
	3	78.2	qd
	4	~41	m
	5	62.4	d
	6	25.3	d
Product of the D281V mutant from [U-^{13}C]MVA-5-PP	1	179.3	d
	2	~49	m
	3	78.2	qd
	4	~41	m
	5	62.4	d
	6	25.3	d

[a] The following abbreviations are used: d, doublet; q, quartet; dd, doublet doublet; qd, quartet doublet; m, multiplet.

$H]^-$, and $[M - H_3PO_4 - {}^{13}CO_2 - H]^-$, respectively (Fig. 8*F*). Almost the same results were obtained with the ESI-MS analyses of the product from the reaction with the D281V mutant (data not shown). These data from the NMR and MS analyses demonstrate that the product from the reaction with the D281T or D281V mutant was MVA-3-P-5-PP, which was predicted to be the intermediate of the DMD reaction, but as of now it has not been detected. Furthermore, it should be emphasized that the replacement of Asp-281 with less polar amino acids did not block the former phosphotransfer step but the latter phosphate-elimination/decarboxylation process of the DMD reaction.

Mutation Analyses of TacM3K—We also tried the mutagenesis on TacM3K to convert the enzyme into decarboxylase. The replacement of Thr-275 in TacM3K with acidic amino acids such as aspartate and glutamate, however, failed to confer decarboxylase activity to the mutants and resulted in complete inactivation (Figs. 4*B* and 5*B*). Because the introduction of such anionic residues alone is supposed to affect the structure of the active site of TacM3K, we also tried to introduce double mutations such as L18K/T275D and L18K/T275E, in which the substituting residues possibly form an ion pair (Fig. 4*B*). The former double mutation mimicked the ion pair between the corresponding residues of SsoDMD, Lys-17 and Asp-281, which held a hydrogen bond distance in the crystal structures of the enzyme, as described above. The double mutants of TacM3K, however, completely lost enzyme activity (data not shown).

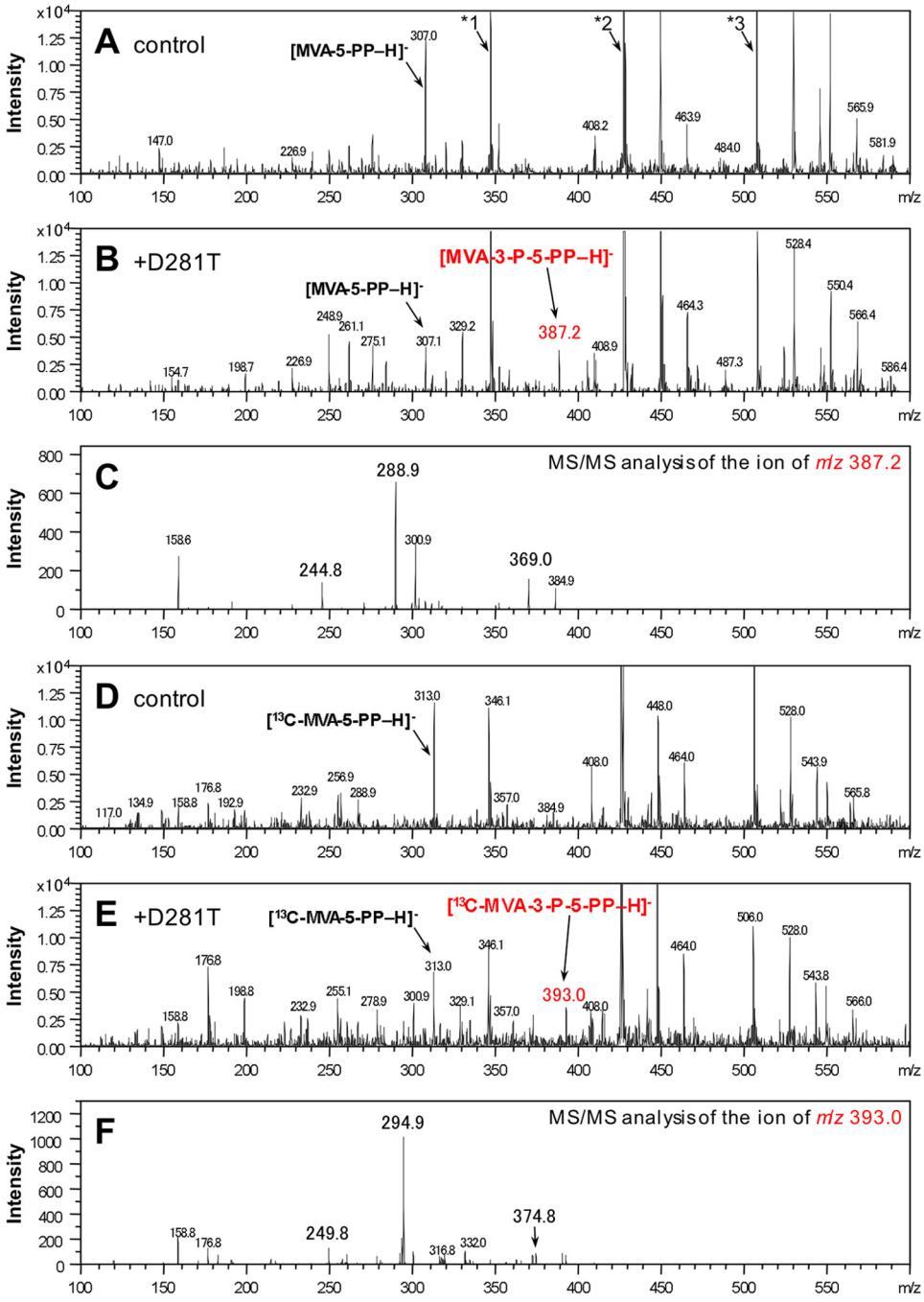

FIGURE 8. **Negative ESI-MS analyses of the product of the D281T mutant from MVA-5-PP.** The samples from the reaction with the non-labeled substrate (*A–C*) or the ^{13}C-labeled substrate (*D* and *E*) were analyzed by ESI-MS. *A* and *D*, negative control; *B* and *E*, the sample after the reaction of the D281T mutant; *C* and *F*, MS/MS analysis of the ion of *m/z* 387.2 and 393.0 from *B* and *E*, respectively. *1, *2, and *3 indicate the ion peaks of $[AMP-H]^-$ (*m/z* ~346), $[ADP-H]^-$ (*m/z* ~426), and $[ATP-H]^-$ (*m/z* ~506), respectively. The reaction with the D281V mutant gave almost the same results as those from the reaction with D281T (data not shown).

Discussion

The expendable nature of the conserved aspartate residue for the initial phosphotransfer step in the DMD reaction, which was suggested by the discovery of M3K, was demonstrated in the present mutagenic study of SsoDMD. The replacement of the Asp-281 residue of SsoDMD with asparagine did not result in a complete loss of DMD activity, which contradicts the role of the aspartate residue as the base catalyst that abstracts a proton from the 3-hydroxyl group of MVA-5-PP. Both the D281T and D281V mutants retained only 3-kinase activity and produced MVA-3-P-5-PP, a hypothetical intermediate of the DMD reaction, which was first proposed by Bloch *et al.* in 1959 (23). The slow release rate of the intermediate, not the genuine product, from the enzyme probably explains the small k_{cat} values of the mutants in comparison with that of the wild type SsoDMD. Compared with the homologous kinase TacM3K, the k_{cat} values of the SsoDMD mutants were also much smaller than the reported k_{cat} of 5.0 s^{-1} of the wild type TacM3K, which was obtained from the reaction with (*R*)-

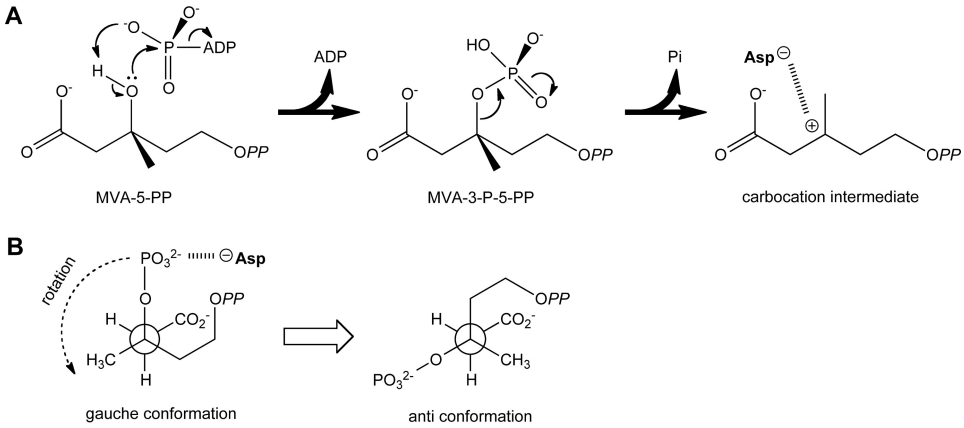

FIGURE 9. **Newly proposed roles of Asp-281 residue in the reaction catalyzed by SsoDMD.** *A,* stabilization of the carbocation intermediate formed by the elimination of inorganic phosphate from MVA-3-P-5-PP. The preceding phosphotransfer reaction from ATP to the non-ionized 3-hydroxyl group of MVA-5-PP is supposedly stimulated by the interactions with Mg^{2+} ion and Lys-190 residue, which are not shown in the figure. *OPP* represents the diphosphate group of MVA-5-PP. *B,* formation of the repulsive force that pushes the 3-phosphate group of MVA-3-P-5-PP away and changes the conformation of the intermediate from gauche to anti.

MVA and ATP (21). In contrast, the K_m values of the mutants for (*RS*)-MVA-5-PP were comparable with the reported K_m value of 97 μM TacM3K for (*R*)-MVA.

These findings also suggest the actual roles of the aspartate residue in the DMD reaction. The most plausible role is the stabilization of an unstable intermediate. As suggested by our theoretical analysis, the γ-phosphate group of ATP is transferred to the protonated 3-hydroxyl group of MVA-5-PP. The release of the phosphate group then generates the 3° carbocation intermediate if the phosphate-elimination/decarboxylation process occurs via the E1 mechanism (Fig. 9*A*). Because the Asp-281 residue interacts closely with its partner Lys-17 residue, its carboxyl group must be unprotonated and can strongly stabilize the proposed carbocation intermediate in a close proximity, supposedly without forming hydrogen bonds. The asparagine residue of the D281N mutant possibly can stabilize the intermediate with its polar amide group, albeit with much lower efficiency, although less polar threonine and valine residues cannot. The lack of a polar residue would make the carbocation intermediate more unstable, causing a significant rise in the activation energy.

Another possible role of the aspartate residue is to change the substrate conformation into one that would be appropriate for E2 elimination in an anti-manner. The involvement of the E1 mechanism in the DMD reaction is supported by the fact that *N*-(carboxymethyl)-*N*-methyldiphosphoethanolamine, an MVA-5-PP analog that mimics the carbocation intermediate, and 6-fluoromevalonate diphosphate, which is supposedly phosphorylated at the 3-hydroxyl group but does not form a destabilized carbocation, potently inhibit DMD in competitive manners (11, 24). Another report, however, has suggested the involvement of the E2 mechanism based on an experiment using *S. pneumoniae* DMD and an MVA-5-PP analog containing a 3-cyclopropyl group in place of the methyl group (10). The authors of that report had expected a rearrangement of the cyclopropyl group to be induced by the formation of the carbocation at C3, but the decarboxylation of the analog occurred without such a rearrangement. Therefore, the authors concluded that the phosphate-elimination/decarboxylation process of DMD occurs in a rather concerted manner, probably developing only a slight positive charge at C3. If that is true, the phosphate and carboxyl groups of MVA-3-P-5-PP must take an "anti"-conformation before their concerted elimination, because the elimination has been proven to occur in an anti-manner via an experiment using substrates stereospecifically labeled with deuterium and tritium (22). The conserved aspartate residue could be involved in the conformational change of the intermediate initiated by the phosphotransfer to the 3-hydroxyl group. The proximity of the negative charges of the aspartate residue and the 3-phosphate group of MVA-3-P-5-PP can result in an impulsive force that can rotate the C–C bonds to induce a change in the conformation of the intermediate from gauche to anti (Fig. 9*B*), although the interaction between the carbocation at C3, which is developed through the E1 mechanism, and the aspartate residue might also cause a similar conformational change.

In contrast to the mutagenesis of SsoDMD and its successful conversion into kinase, the mutations introduced in TacM3K did not confer decarboxylase activity to the mutants. Such artificial MVA decarboxylases, and also undiscovered novel ones, are needed in industry because the direct decarboxylation of MVA yields isoprenol, which is one of the candidates for the next generation of biofuels. Recently, a P450 fatty acid decarboxylase from the *Jeotgalicoccus* sp., which was proposed to form a carbocation intermediate like DMD, was reported to have considerable activity toward MVA (25). Further understanding of the catalytic and substrate-recognition mechanisms of DMD and M3K, however, will help create mutants from them possessing high MVA decarboxylase activity.

Experimental Procedures

Materials—Partisil K6F normal phase precoated TLC plates were purchased from Merck Millipore, Darmstadt, Germany. The radiolabeled substrates, [2-^{14}C]MVA-5-P (55Ci/mol) and [1-^{14}C]IPP (55Ci/mol), were purchased from American Radiolabeled Chemicals. [U-^{13}C]MVA was prepared as described elsewhere (26).

General Procedures—Restriction enzyme digestions, transformations, and other standard molecular biological techniques were carried out as described by Sambrook *et al.* (27).

Recombinant Expression and Purification of Enzymes—For the expression of MVK and PMK from *S. solfataricus* and of SsoDMD, *E. coli* Rosetta (DE3) transformed with pET16b-SsoMVK, -SsoPMK, and -SsoDMD, respectively, was used as described in our previous papers (28). For the expression of TacM3K, *E. coli* Rosetta (DE3) harboring the pET15b plasmid containing the *ta1305* gene (pET15b-TacM3K) was used as described elsewhere (20). Partial purification of the enzymes was performed by affinity chromatography using a 1-ml His-Trap FF crude column (GE Healthcare), as described previously (20, 28). Their purity was confirmed by SDS-PAGE.

X-ray Crystallographic Analysis of the Complex Structures of SsoDMD—Recombinant expression and purification for the crystallization of SsoDMD were performed as described in our previous study (17). The purified recombinant SsoDMD was crystallized at 20 °C using the hanging-drop vapor diffusion method. The reservoir solution for crystallization was 0.1 M sodium acetate, pH 4.6, containing 1.5 M ammonium sulfate. The volume of the reservoir solution was 100 μl, and drops were prepared by mixing 2 μl of the purified enzyme solution of >20 mg/ml, 2 μl of the reservoir solution, 0.2 μl of 100 mM MVA-5-PP, 0.2 μl of 100 mM $MgCl_2$, and either 0.2 μl of 100 mM ATPγS for SsoDMD·ATPγS·MVA-5-PP or 100 mM ADP for SsoDMD·ADP·MVA-5-PP. After crystals were grown, the reservoir solution was exchanged with 100 μl of 0.1 M sodium acetate, pH 4.6, which contained 3.0 M ammonium sulfate for cryoprotection. After 2 weeks of equilibration, the crystals were used for X-ray data collection. Diffraction data from the crystals of SsoDMD·ATPγS·MVA-5-PP and SsoDMD·ADP·MVA-5-PP were collected via beamlines BL-17A and AR-NW12A, respectively, at the Photon Factory, Tsukuba, Japan. The data set from the crystal of SsoDMD·ADP·MVA-5-PP was processed and scaled using the CCP4 programs (29), Mosflm (30), and SCALA (31), respectively, and that from the crystal of SsoDMD·ATPγS·MVA-5-PP was processed and scaled using HKL2000 (32). The data sets, belonged to space groups H32, were used for phase calculation via a molecular replacement method, in which the BALBES program (33) automatically performed the calculation with a series of search models that have a sequence homology with SsoDMD. Finally, using the substrate-free structure of SsoDMD (PDB code 4Z7Y) (17) as search models for the calculation, we obtained the correct phases. The structures were built using the ARP/wARP (34) and COOT (35) programs and were refined using Refmac (36), with 5% of the data set aside as a free set. Models of AMP, ADP, ATPγS, MVA-5-PP, and sulfate were placed based on different electron density maps. The final model, composed of residues ranging from 1 (SsoDMD·ATPγS·MVA-5-PP) or 2 (SsoDMD·ADP·MVA-5-PP) to 325, agreed with the crystallographic data with values for R_{work} and R_{free} of 16.5 and 19.2% (SsoDMD·ATPγS·MVA-5-PP) and 16.9 and 20.2% (SsoDMD·ADP·MVA-5-PP), respectively (Table 1). All figures were produced using PyMOL software.

Atomic Coordinates and Charges—As a basis for the computations, the crystal structure of SsoDMD·ATPγS·MVA-5-PP at resolutions of 1.5 Å (PDB code 5GMD) were used. The positions of the hydrogen atoms were energetically optimized with CHARMM (37) by using the CHARMM22 force field. During this procedure, the positions of all non-hydrogen atoms were fixed, and the standard charge states of all the titratable groups were maintained, *i.e.* basic and acidic groups were considered to be protonated and deprotonated, respectively. Sulfur atoms in ATPγS were replaced with oxygen atoms. The position of the replaced oxygen atoms in ATPγS were energetically optimized with CHARMM (37) by using the CHARMM22 force field. All the other atoms with coordinates available in the crystal structure were not geometrically optimized.

Atomic partial charges of the amino acids were adopted from the all-atom CHARMM22 (37) parameter set. The triphosphoric part of ATP was treated as a titratable site. The charges of the adenosine part of ATP was adopted from the all-atom CHARMM22 parameter set by referring to the adenosine charge of the ATP in CHARMM. MVA-5-PP was treated as being composed of three independent carboxylic, hydroxyl, and diphosphoric titratable sites. For the carboxylic titratable site, we prepared for both protonated and deprotonated states of the charges by referring to the carboxylic groups in CHARMM.

For the triphosphoric and diphosphoric parts, we prepared for deprotonated and protonated states ($[PPP]^{4-}$-/$[H\text{-}PPP]^{3-}$-/$[H_2\text{-}PPP]^{2-}$-, and $[PP]^{3-}$-/$[H\text{-}PP]^{2-}$-/$[H_2\text{-}PP]^{-}$-) of the charges (supplemental Tables S1 and S2, respectively). For the hydroxyl titratable site, we also prepared for both protonated and deprotonated states of the charges (supplemental Table S3). The charges were determined from the electronic wave functions by fitting the resultant electrostatic potential in the neighborhood of these molecules by using the restrained electrostatic potential procedure (38). The electronic wave functions were calculated using the density functional (DFT) module in Jaguar version 7.7 (39) and the B3LYP functional with the 6–31G** basis sets.

Protonation Pattern and pK_a—The present computation is based on the electrostatic continuum model created by solving the linear Poisson-Boltzmann equation with the MEAD program (40). To obtain the absolute pK_a values of target sites, we calculated the difference in the electrostatic energy between the protonated and deprotonated states in a reference model system using a known experimentally measured pK_a value. The difference in the pK_a value of the protein relative to the reference system was added to the known reference pK_a value. The experimentally measured pK_a values employed as references were 4.0 for the carboxylic site of MVA-5-PP (≈Asp), 16.5 for the hydroxyl site of MVA-5-PP (≈*tert*-butyl alcohol) (41), 5.77 for $[PP]^{3-}$-/$[H\text{-}PP]^{2-}$-, and 1.49 for $[H\text{-}PP]^{2-}$-/$[H_2\text{-}PP]^{-}$- of MVA-5-PP (42), 6.26 for $[PPP]^{4-}$-/$[H\text{-}PPP]^{3-}$- and 2.30 for $[H\text{-}PPP]^{3-}$-/$[H_2\text{-}PPP]^{2-}$- of ATP (43) 12.0 for Arg, 4.0 for Asp, 9.5 for Cys, 4.4 for Glu, 10.4 for Lys, 9.6 for Tyr (44), and 7.0 and 6.6 for the Nε and Nδ atoms of His, respectively (45–47).

All other titratable sites were fully equilibrated to the protonation state of the target site during the titration. The ensemble of the protonation patterns was sampled using the Monte Carlo method of Karlsberg (48). The dielectric constants were set to $\epsilon_p = 4$ inside the protein and $\epsilon_w = 80$ for water. All computations were performed at 300 K, pH 7.0, and an ionic strength of

100 mM. The linear Poisson-Boltzmann equation was solved using a three-step grid-focusing procedure at resolutions of 2.5, 1.0, and 0.3 Å. Monte Carlo sampling yielded the probabilities of the two protonation states of the molecule ([protonated] and [deprotonated]). The pK_a value was evaluated using the Henderson-Hasselbalch equation. A bias potential was applied to obtain an equal amount of both protonation states ([protonated] = [deprotonated]), yielding the pK_a value as the resultant bias potential.

Site-directed Mutagenesis—The SsoDMD mutants, D281N, D281T, and D281V, along with the TacM3K mutants, T275D, T275E, L18K/T275D, and L18K/T275E, were generated using a QuikChange mutagenesis kit (Stratagene) with either pET16b-SsoDMD or pET15b-TacM3K as a template, respectively, and the oligonucleotide primers designed appropriately. The sequences of the mutants were confirmed by DNA sequencing. The recombinant expression and purification of the mutants were performed by the same methods used for the wild type enzymes.

Preparation of ^{14}C-Labeled Substrates—[2-^{14}C]MVA and [2-^{14}C]MVA-5-PP were enzymatically synthesized from [2-^{14}C]MVA-5-P using Antarctic phosphatase (New England Biolabs) and recombinant *S. solfataricus* PMK, respectively, as described in our previous work (28).

Radio-TLC Analysis of the Reaction Products—To analyze the products from SsoDMD and TacM3K mutants, 25 μl of a reaction solution containing 25 pmol of the ^{14}C-labeled substrate ([2-^{14}C]MVA, [2-^{14}C]MVA-5-P, or [2-^{14}C]MVA-5-PP), 25 pmol (~1 μg) of the purified recombinant SsoDMD, 100 nmol of ATP, 1 μmol of sodium phosphate buffer, pH 7.5, and 125 nmol of $MgCl_2$ was prepared. After reaction for 15 min at 60 °C, 10 μl of the solution was spotted on a Partisil K6F normal phase TLC plate, and the plate was developed with *n*-propanol, 28% ammonium water, H_2O (6:3:1). To roughly compare the enzyme activities of the wild type and the D281T and D281V mutants of SsoDMD, 2.5, 25, or 250 ng of the enzymes was used for the reaction.

ADP Coupling Assays of the DMD Mutants—For kinetic analyses, ATP-dependent kinase activity of the SsoDMD mutants was assayed via a rate measurement of the formation of ADP, which was coupled to the oxidation of NADH to NAD^+ via pyruvate kinase from rabbit muscle (Oriental Yeast Co.) and lactate dehydrogenase from pig heart (Oriental Yeast Co.). Then, various amounts of (*RS*)-MVA-5-PP from 10 to 250 nmol were added to the reaction solution containing 36.5 μmol of sodium phosphate buffer, pH 7.5, along with 80 nmol of NADH, 2.5 μmol of $MgCl_2$, 2 μmol of ATP, 2.5 μmol of phosphoenolpyruvate, 5 units of pyruvate kinase, and 5 units of lactate dehydrogenase. After preincubation of the solution at 55 °C for 15 min, the reaction at the same temperature was started with the addition of either 0.37 μg of the wild type or 11.8 μg of either the D281T or D281V mutant of SsoDMD in a total volume of 500 μl. The time course of a decrease in absorbance of 340 nm due to the oxidation of NADH was measured by UV spectrophotometer (UV-2450, Shimadzu). It was confirmed that the pyruvate kinase and lactate dehydrogenase from the animal origins retained enough activities through the high temperature incubation process. The initial reaction rates of the enzymes were calculated from the linear range of the change in absorbance, using an extinction coefficient of NADH, 6.22 mM^{-1} cm^{-1}. Kinetic parameters were obtained by fitting a Michaelis-Menten curve to each data set using KaleidaGraph (Synergy software).

NMR Analysis of the ^{13}C-Labeled Products—In a volume of 300 μl, a reaction mixture containing 1.95 μmol of [U-^{13}C]MVA, 9 nmol of *S. solfataricus* MVK, 6 nmol of *S. solfataricus* PMK, 30 μmol of sodium phosphate buffer, pH 7.5, 7.5 μmol of ATP, 0.3 μmol of $MgCl_2$, and 10% D_2O was prepared for the first reaction and incubated at 60 °C for 2 h. After filtration using a 10-kDa cutoff spin column filter (Vivaspin 500, GE Healthcare), 275 μl of the filtrate was used for the second reaction. Subsequently, 60 nmol of an SsoDMD mutant, either D281T or D281V, and 15 μmol of ATP were added to the filtrate. The volume of the solution was adjusted using a 9:1 mixture of H_2O/D_2O to 600 μl, and the second reaction was conducted at 60 °C for 3 h. After filtration, the ^{13}C NMR spectrum of the product from the second reaction was analyzed by an AVANCE III HD 600 NMR spectrometer equipped with a cryoprobe (Bruker). As a negative control, the same volume of water was added in place of the enzymes.

MS Analysis of the Products—In a 200-μl volume, 1 μmol of non-labeled MVA or [U-^{13}C]MVA was reacted with 3 nmol of *S. solfataricus* MVK and 2 nmol of *S. solfataricus* PMK at 60 °C for 2 h in 20 μmol of ammonium acetate buffer, pH 7.0, containing 5 μmol of ATP and 0.2 μmol of $MgCl_2$. After filtration with a Vivaspin 500 filter (10-kDa molecular mass cutoff), a 175-μl volume of the filtrate was reacted in a total volume of 200 μl with 3 nmol of SsoDMD mutants, either D281T or D281V, at 60 °C for 3 h. As a negative control, the same volume of water was added in place of the enzymes. After filtration with a Vivaspin 500 filter (10-kDa molecular mass cutoff), a 175-μl volume of the filtrate was diluted with the same volume of acetonitrile and analyzed by negative ion ESI-MS with an Esquire 3000 mass spectrometer (Bruker) by direct infusion.

Author Contributions—H. H. and T. Y. designed the study. H. H., K. M., H. U., and H. I. wrote the manuscript. A. H. crystallized DMD. H. U. determined crystal structures. T. T. and H. I. performed energetics calculation. K. M. and A. H. constructed and characterized the mutant enzymes. K. M. determined the structure of the products of the D281T and D281N mutants by NMR and ESI-MS. H. K. prepared [U-^{13}C]MVA. All authors analyzed the results and approved the final version of the manuscript.

Acknowledgments—Theoretical calculations were partly performed using the Research Center for Computational Science, Okazaki, Japan. We are grateful to Kazushi Koga, Nagoya University, for help with the NMR analysis.

References

1. Kuzuyama, T., Hemmi, H., and Takahashi, S. (2010) in *Comprehensive Natural Products II Chemistry and Biology* (Mander, L., and Liu, H.-W., eds) pp. 493–516, Elsevier, Oxford, United Kingdom
2. Miziorko, H. M. (2011) Enzymes of the mevalonate pathway of isoprenoid biosynthesis. *Arch. Biochem. Biophys.* **505,** 131–143
3. Li, T., Huo, L., Pulley, C., and Liu, A. (2012) Decarboxylation mechanisms in biological system. *Bioorg. Chem.* **43,** 2–14
4. Froese, D. S., Forouhar, F., Tran, T. H., Vollmar, M., Kim, Y. S., Lew, S., Neely, H., Seetharaman, J., Shen, Y., Xiao, R., Acton, T. B., Everett, J. K., Cannone, G., Puranik, S., Savitsky, P., *et al.* (2013) Crystal structures of

malonyl-coenzyme A decarboxylase provide insights into its catalytic mechanism and disease-causing mutations. *Structure* **21,** 1182–1192
5. Bertoldi, M. (2014) Mammalian dopa decarboxylase: structure, catalytic activity and inhibition. *Arch. Biochem. Biophys.* **546,** 1–7
6. Kutter, S., Wille, G., Relle, S., Weiss, M. S., Hübner, G., and König, S. (2006) The crystal structure of pyruvate decarboxylase from *Kluyveromyces lactis.* Implications for the substrate activation mechanism of this enzyme. *FEBS J.* **273,** 4199–4209
7. Payne, K. A., White, M. D., Fisher, K., Khara, B., Bailey, S. S., Parker, D., Rattray, N. J., Trivedi, D. K., Goodacre, R., Beveridge, R., Barran, P., Rigby, S. E., Scrutton, N. S., Hay, S., and Leys, D. (2015) New cofactor supports α,β-unsaturated acid decarboxylation via 1,3-dipolar cycloaddition. *Nature* **522,** 497–501
8. Dellas, N., Thomas, S. T., Manning, G., and Noel, J. P. (2013) Discovery of a metabolic alternative to the classical mevalonate pathway. *eLife* **2,** e00672
9. VanNice, J. C., Skaff, D. A., Keightley, A., Addo, J. K., Wyckoff, G. J., and Miziorko, H. M. (2014) Identification in *Haloferax volcanii* of phosphomevalonate decarboxylase and isopentenyl phosphate kinase as catalysts of the terminal enzymatic reactions in an archaeal alternate mevalonate pathway. *J. Bacteriol.* **196,** 1055–1063
10. Lefurgy, S. T., Rodriguez, S. B., Park, C. S., Cahill, S., Silverman, R. B., and Leyh, T. S. (2010) Probing ligand-binding pockets of the mevalonate pathway enzymes from *Streptococcus pneumoniae. J. Biol. Chem.* **285,** 20654–20663
11. Dhe-Paganon, S., Magrath, J., and Abeles, R. H. (1994) Mechanism of mevalonate pyrophosphate decarboxylase: evidence for a carbocationic transition state. *Biochemistry* **33,** 13355–13362
12. Bonanno, J. B., Edo, C., Eswar, N., Pieper, U., Romanowski, M. J., Ilyin, V., Gerchman, S. E., Kycia, H., Studier, F. W., Sali, A., and Burley, S. K. (2001) Structural genomics of enzymes involved in sterol/isoprenoid biosynthesis. *Proc. Natl. Acad. Sci. U.S.A.* **98,** 12896–12901
13. Byres, E., Alphey, M. S., Smith, T. K., and Hunter, W. N. (2007) Crystal structures of *Trypanosoma brucei* and *Staphylococcus aureus* mevalonate diphosphate decarboxylase inform on the determinants of specificity and reactivity. *J. Mol. Biol.* **371,** 540–553
14. Voynova, N. E., Fu, Z., Battaile, K. P., Herdendorf, T. J., Kim, J. J., and Miziorko, H. M. (2008) Human mevalonate diphosphate decarboxylase: characterization, investigation of the mevalonate diphosphate binding site, and crystal structure. *Arch. Biochem. Biophys.* **480,** 58–67
15. Barta, M. L., McWhorter, W. J., Miziorko, H. M., and Geisbrecht, B. V. (2012) Structural basis for nucleotide binding and reaction catalysis in mevalonate diphosphate decarboxylase. *Biochemistry* **51,** 5611–5621
16. Barta, M. L., Skaff, D. A., McWhorter, W. J., Herdendorf, T. J., Miziorko, H. M., and Geisbrecht, B. V. (2011) Crystal structures of *Staphylococcus epidermidis* mevalonate diphosphate decarboxylase bound to inhibitory analogs reveal new insight into substrate binding and catalysis. *J. Biol. Chem.* **286,** 23900–23910
17. Hattori, A., Unno, H., Goda, S., Motoyama, K., Yoshimura, T., and Hemmi, H. (2015) *In vivo* formation of the protein disulfide bond that enhances the thermostability of diphosphomevalonate decarboxylase, an intracellular enzyme from the hyperthermophilic archaeon *Sulfolobus solfataricus. J. Bacteriol.* **197,** 3463–3471
18. Krepkiy, D., and Miziorko, H. M. (2004) Identification of active site residues in mevalonate diphosphate decarboxylase: implications for a family of phosphotransferases. *Protein Sci.* **13,** 1875–1881
19. Vinokur, J. M., Korman, T. P., Sawaya, M. R., Collazo, M., Cascio, D., and Bowie, J. U. (2015) Structural analysis of mevalonate-3-kinase provides insight into the mechanisms of isoprenoid pathway decarboxylases. *Protein. Sci.* **24,** 212–220
20. Azami, Y., Hattori, A., Nishimura, H., Kawaide, H., Yoshimura, T., and Hemmi, H. (2014) (*R*)-Mevalonate 3-phosphate is an intermediate of the mevalonate pathway in *Thermoplasma acidophilum*. *J. Biol. Chem.* **289,** 15957–15967
21. Vinokur, J. M., Korman, T. P., Cao, Z., and Bowie, J. U. (2014) Evidence of a novel mevalonate pathway in archaea. *Biochemistry* **53,** 4161–4168
22. Cornforth, J. W., Cornforth, R. H., Popják, G., and Yengoyan, L. (1966) Studies on the biosynthesis of cholesterol. XX. Steric course of decarboxylation of 5-pyrophosphomevalonate and of the carbon to carbon bond formation in the biosynthesis of farnesyl pyrophosphate. *J. Biol. Chem.* **241,** 3970–3987
23. Bloch, K., Chaykin, S., Phillips, A. H., and De Waard, A. (1959) Mevalonic acid pyrophosphate and isopentenyl pyrophosphate. *J. Biol. Chem.* **234,** 2595–2604
24. Nave, J. F., d'Orchymont, H., Ducep, J. B., Piriou, F., and Jung, M. J. (1985) Mechanism of the inhibition of cholesterol biosynthesis by 6-fluoromevalonate. *Biochem. J.* **227,** 247–254
25. Yang, J., Nie, Q., Liu, H., Xian, M., and Liu, H. (2016) A novel MVA-mediated pathway for isoprene production in engineered *E. coli*. *BMC Biotechnol.* 16:5
26. Sugai, Y., Miyazaki, S., Mukai, S., Yumoto, I., Natsume, M., and Kawaide, H. (2011) Enzymatic total synthesis of gibberellin A_4 from acetate. *Biosci. Biotechnol. Biochem.* **75,** 128–135
27. Sambrook, J., Fritsch, E. F., and Maniatis, T. (1989) *Molecular Cloning: A Laboratory Manual*, 2nd ed., Cold Spring Harbor Laboratory Press, Cold Spring Harbor, NY
28. Nishimura, H., Azami, Y., Miyagawa, M., Hashimoto, C., Yoshimura, T., and Hemmi, H. (2013) Biochemical evidence supporting the presence of the classical mevalonate pathway in the thermoacidophilic archaeon *Sulfolobus solfataricus*. *J. Biochem.* **153,** 415–420
29. Collaborative and Computational Project, Number 4 (1994) The CCP4 suite: Programs for protein crystallography. *Acta Crystallogr. D Biol. Crystallogr.* **50,** 760–763
30. Leslie, A. G. (2006) The integration of macromolecular diffraction data. *Acta Crystallogr. D Biol. Crystallogr.* **62,** 48–57
31. Evans, P. (2006) Scaling and assessment of data quality. *Acta Crystallogr. D Biol. Crystallogr.* **62,** 72–82
32. Otwinowski, Z., and Minor, W. (1997) Processing of X-ray diffraction data collected in oscillation mode. *Methods Enzymol.* **276,** 307–326
33. Long, F., Vagin, A. A., Young, P., and Murshudov, G. N. (2008) BALBES: A molecular-replacement pipeline. *Acta Crystallogr. D Biol. Crystallogr.* **64,** 125–132
34. Langer, G., Cohen, S. X., Lamzin, V. S., and Perrakis, A. (2008) Automated macromolecular model building for X-ray crystallography using ARP/wARP version 7. *Nat. Protocols* **3,** 1171–1179
35. Emsley, P., and Cowtan, K. (2004) Coot: Model-building tools for molecular graphics. *Acta Crystallogr. D Biol. Crystallogr.* **60,** 2126–2132
36. Murshudov, G. N., Skubák, P., Lebedev, A. A., Pannu, N. S., Steiner, R. A., Nicholls, R. A., Winn, M. D., Long, F., and Vagin, A. A. (2011) REFMAC5 for the refinement of macromolecular crystal structures. *Acta Crystallogr. D Biol. Crystallogr.* **67,** 355–367
37. Brooks, B. R., Bruccoleri, R. E., Olafson, B. D., States, D. J., Swaminathan, S., and Karplus, M. (1983) CHARMM: A program for macromolecular energy, minimization, and dynamics calculations. *J. Comput. Chem.* **4,** 187–217
38. Bayly, C. I., Cieplak, P., Cornell, W. D., and Kollman, P. A. (1993) A well-behaved electrostatic potential based method using charge restraints for deriving atomic charges: the RESP model. *J. Phys. Chem.* **97,** 10269–10280
39. Bochevarov, A. D., Harder, E., Hughes, T. F., Greenwood, J. R., Braden, D. A., Philipp, D. M., Rinaldo, D., Halls, M. D., Zhang, J., and Friesner, R. A. (2013) Jaguar: a high-performance quantum chemistry software program with strengths in life and materials sciences. *Int. J. Quantum Chem.* **113,** 2110–2142
40. Bashford, D., and Karplus, M. (1990) pK_a's of ionizable groups in proteins: atomic detail from a continuum electrostatic model. *Biochemistry* **29,** 10219–10225
41. Reeve, W., Erikson, C. M., and Aluotto, P. F. (1979) New method for the determination of the relative acidities of alcohols in alcoholic solutions. Nucleophilicities and competitive reactivities of alkoxides and phenoxides. *Can. J. Chem.* **57,** 2747–2754
42. Styer, L. (1988) in *Biochemistry,* 3rd ed., p. 1046, W. H. Freeman, New York
43. Bjerrum, J., Schwarzenbach, G., and Sillén, L. G. (1958) *Stability Constants*, Chemical Society, London

44. Nozaki, Y., and Tanford, C. (1967) Acid-base titrations in concentrated guanidine hydrochloride. Dissociation constants of guanidinium ion and of some amino acids. *J. Am. Chem. Soc.* **89,** 736–742
45. Tanokura, M. (1983) ^{1}H nuclear magnetic-resonance titration curves and microenvironments of aromatic residues in bovine pancreatic ribonuclease A. *J. Biochem.* **94,** 51–62
46. Tanokura, M. (1983) ^{1}H NMR study on the tautomerism of the imidazole ring of histidine residues: II. Microenvironments of histidine-12 and histidine-119 of bovine pancreatic ribonuclease A. *Biochim. Biophys. Acta* **742,** 586–596
47. Tanokura, M. (1983) ^{1}H NMR study on the tautomerism of the imidazole ring of histidine residues: I. Microscopic p*K* values and molar ratios of tautomers in histidine-containing peptides. *Biochim. Biophys. Acta* **742,** 576–585
48. Rabenstein, B., and Knapp, E. W. (2001) Calculated pH-dependent population and protonation of carbon-monoxy-myoglobin conformers. *Biophys. J.* **80,** 1141–1150

A Single Amino Acid Mutation Converts (*R*)-5-Diphosphomevalonate Decarboxylase into a Kinase

Kento Motoyama, Hideaki Unno, Ai Hattori, Tomohiro Takaoka, Hiroshi Ishikita, Hiroshi Kawaide, Tohru Yoshimura and Hisashi Hemmi

J. Biol. Chem. 2017, 292:2457-2469.
doi: 10.1074/jbc.M116.752535 originally published online December 21, 2016